

Article

Performance Evaluation and Durability Analysis of NiFeCoO_x Catalysts for Alkaline Water Electrolysis in Anion Exchange Membrane Electrolyzers

Khaja Wahab Ahmed * and Michael Fowler *

Department of Chemical Engineering, University of Waterloo, Waterloo, ON N2L 3G1, Canada

* Correspondence: kwahmed@uwaterloo.ca (K.W.A.); mfowler@uwaterloo.ca (M.F.);

Tel.: +1-519-888-4567 (ext. 33415) (M.F.)

Abstract: This study examines the catalytic activity of NiFeCoO_x catalysts for anion exchange membrane (AEM) water electrolysis. The catalysts were synthesized with a Ni to Co ratio of 2:1 and Fe content ranges from 2.5 to 12.5 wt%. The catalysts were characterized using scanning electron microscopy (SEM) and X-ray diffraction (XRD) techniques. The catalytic activity of the NiFeCoO_x catalysts was evaluated through linear sweep voltammetry (LSV) and chronoamperometry (CA) experiments for the oxygen evolution reaction (OER). The catalyst with 5% Fe content exhibited the highest catalytic activity, achieving an overpotential of 228 mV at a current density of 10 mA cm⁻². Long-term catalyst testing for the OER at 50 mA cm⁻² showed stable electrolysis operation for 100 h. The catalyst was further analyzed in an AEM water electrolyzer in a single-cell test, and the NiFeCoO_x catalyst with 5% Fe at the anode demonstrated the highest current densities of 1516 mA cm⁻² and 1620 mA cm⁻² at 55 °C and 70 °C at 2.1 V. The maximum current density of 1880 mA cm⁻² was achieved at 2.2 V and 70 °C. The Nyquist plot analysis of electrolysis at 55 °C showed that the NiFeCoO_x catalyst with 5% Fe had lower activation resistance compared with the other Fe loadings, indicating enhanced performance. The durability test was performed for 8 h, showing stable AEM water electrolysis with minimum degradation. An overall cell efficiency of 70.5% was achieved for the operation carried out at a higher current density of 0.8 A cm⁻².



Citation: Ahmed, K.W.; Fowler, M. Performance Evaluation and Durability Analysis of NiFeCoO_x Catalysts for Alkaline Water Electrolysis in Anion Exchange Membrane Electrolyzers. *Catalysts* **2024**, *14*, 322. <https://doi.org/10.3390/catal14050322>

Academic Editor: Carlo Santoro

Received: 12 April 2024

Revised: 5 May 2024

Accepted: 8 May 2024

Published: 14 May 2024



Copyright: © 2024 by the authors. Licensee MDPI, Basel, Switzerland. This article is an open access article distributed under the terms and conditions of the Creative Commons Attribution (CC BY) license (<https://creativecommons.org/licenses/by/4.0/>).

Keywords: AEM; PEM; OER; EIS; ohmic resistance

1. Introduction

Because of global warming and climate change issues, there is a need to switch from fossil fuels to renewable energy sources. Hydrogen is considered the fuel for the future and can reduce carbon emissions and pollution caused by fossil fuels [1,2]. Hydrogen can be used to generate electricity using fuel cells, and the only by-product is water. Proton exchange membrane (PEM) electrolyzers are very effective in producing hydrogen because of their compact size, high current densities, and high-purity hydrogen at high pressures. The widespread use of PEM electrolyzers is limited due the use of expensive and rare elements as catalysts, as IrO₂ is used for the oxygen evolution reaction (OER) and Pt for the hydrogen evolution reaction (HER) [3,4].

Anion exchange membrane (AEM) water electrolyzers share a similar design to PEM electrolyzers. AEM electrolyzers utilize a thin polymeric anion exchange membrane that separates the anode and cathode sides and transports the hydroxyl ions [5]. Unlike alkaline electrolyzers, AEM electrolyzers do not use any diaphragm and minimize gas crossover [6]. Compared with commercial alkaline electrolyzers, AEM water electrolyzers can be used at low concentrations of electrolytes, and it is also possible to operate them with distilled water [7]. Non-precious transition metal oxide catalysts such as Ni- and Co-based oxides can be used in these electrolyzers because of the relative stability and activity of these catalysts in alkaline conditions [8].

In water electrolysis, the oxygen evolution reaction (OER) is considered kinetically more demanding compared with the hydrogen evolution reaction (HER). The overpotential of the OER is higher than the HER. The OER mechanism involves several intermediate steps, which are kinetically demanding because they require four electrons for the evolution of a molecule of oxygen. OER catalysis is an active research area that is focused on decreasing the overpotential of the reaction [9,10]. There is a need to have active OER catalysts with the least overpotential to improve AEM water electrolyzer performance and efficiency.

With the advancement in AEM, more research is now focused on nonprecious OER catalysts for AEM water electrolyzers and AEM fuel cells. Three main classes of OER catalysts have been widely studied for the OER, which are spinels such as NiFe_2O_4 , perovskites such as SrCoO_3 , and mixed metal oxide catalysts such as LaNiCoO_x [11–13]. It was reported that a spinel catalyst's structure that contains Ni and Fe has higher OER activity. This is because Ni and Fe can have synergistic effects on the OER process, resulting in improved activity compared with catalysts containing only one of these elements. Several studies have identified Ni-Fe spinel compounds as promising electrocatalysts for the OER [13–15].

The addition of Fe is reported to stabilize Ni in the Ni^{2+} form in Ni-Fe OER catalysts [16]. Mixed oxide catalysts containing both Ni and Fe have been found to have greatly increased OER activity compared with pure Ni electrodes or other bimetallic mixed oxides. The modification of a Ni-Fe bimetallic catalyst with a third metal has shown higher activity compared with a bimetallic OER catalyst [17–19]. The activity of monometallic metal oxide films for the oxygen evolution reaction (OER) can vary depending on the specific metal used. Previous studies have suggested that nickel (Ni) is the most active of the group 3d metals for the OER [20]. More recent research has indicated that the high apparent activity of Ni oxide samples may be due to contamination with trace amounts of iron (Fe) [21]. In addition, layered double hydroxides (LDHs) have been shown to have higher electrochemical properties, and NiCo LDH is reported to have enhanced performance along with morphological changes because of the addition of a third metal [22].

In this work, NiFeCoO_x mixed metal oxides were synthesized with increasing Fe content. The activity of these catalysts was tested in a three-electrode system and in an AEM electrolyzer for water electrolysis. The AEM electrolyzer operation was also analyzed by electrochemical impedance spectroscopy (EIS) with NiFeCoO_x catalysts at the anode. In addition, a NiFeCo(OH)_x catalyst was also synthesized, and the activity was compared with the NiFeCoO_x catalyst. The catalyst durability was also tested in the three-electrode system and the AEM electrolyzer.

2. Results

The morphology of the nickel foam and GDL was analyzed by scanning electron microscopy (SEM, Leo 1550, Zeiss, Dublin, CA, USA). Figure 1a,b show the nickel foam without any catalyst coating, which shows pore size ranges of 100 to 500 μm . Figure 1c illustrates a cross-sectional view of the nickel foam coated with the NiFeCoO_x catalyst. It shows a thin layer of the catalyst on the surface of the nickel foam. The thickness of the GDE is around 790 μm , and the cross-sectional image shows that the top surface of the GDE is covered with the catalyst layer, and, because of the applied pressure during the fabrication process, particles are also deposited within the structure of nickel foam. SEM results of NiFeCoO_x (5% Fe) and NiFeCo(OH)_x (5%Fe) are shown in Figure S1, which indicate that NiFeCoO_x and NiFeCo(OH)_x had particle sizes in the micrometer range.

Figure 1d shows the Pt/C-coated carbon paper cathode. The total loading of the catalyst was 1 mg/cm^2 of Pt, and it covered the carbon paper completely. There are some cracks that are due to the heat treatment during the deposition of the catalyst. Figure 1e shows the Energy-dispersive X-ray spectroscopy (EDS) spectra of NiFeCoO_x 5 wt% catalyst, which confirms the ratio of Ni to Co and a Fe content of 5 wt% with respect to the total metal content of the catalyst. Figures S2–S6 show the EDS spectrum of the NiFeCoO_x catalyst series. All the EDS results confirmed the total Fe content in each catalyst.

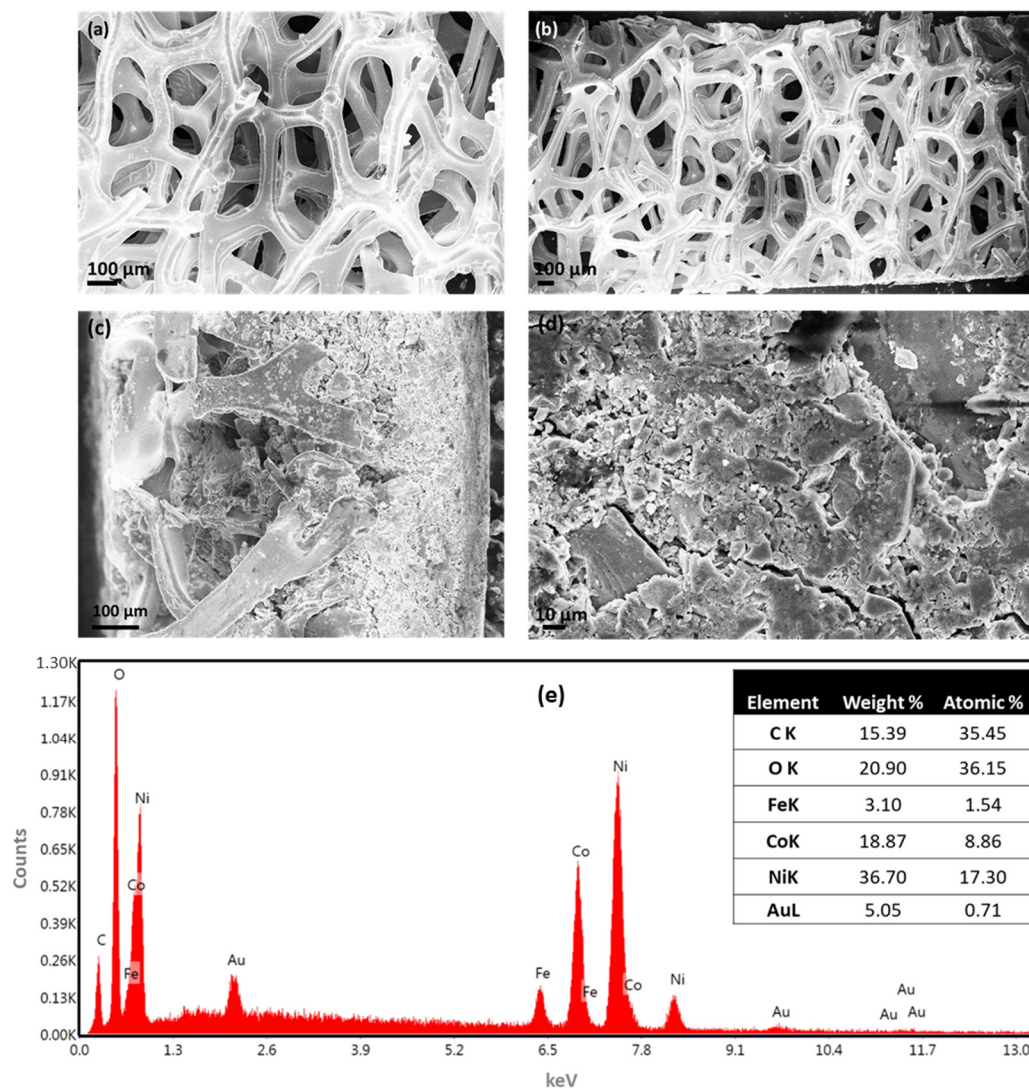


Figure 1. SEM of (a,b) the nickel foam without any catalyst deposition, (c) a cross-sectional image of the NiFeCoO_x (5% Fe) catalyst layer deposited on the nickel foam, (d) Pt/C coated on carbon paper, and (e) EDS of the NiFeCoO_x (5% Fe) catalyst.

X-ray diffraction (XRD) investigations were carried out using a Rigaku Miniflex 600 instrument, employing Cu-K α radiation with a wavelength of 1.54184 Å. The XRD of NiFeCoO_x (2.5–12.5 wt.% Fe) catalysts with a Ni-to-Co molar ratio of 2:1 showed a NiCo₂O₄ spinel crystal structure with the most intense peak at 2θ 36.8 assigned to (311), as shown in Figure 2. The peaks were indexed to NiCo₂O₄ (JCPDS card no. 20-0781). Because of the low loading of Fe in NiFeCoO_x catalysts, diffraction peaks for NiFe₂O₄ and Fe₂O₃ were not present. Some peaks corresponding to NiCo₂O₄ were not distinct because of the 2:1 ratio of Ni to Co, indicating the presence of NiO/NiCo₂O₄ phases in the catalyst. In Figure 2, the XRD of NiO is added for comparison, where nickel oxide had five distinct peaks centered at 2θ 37.36, 43.36, 60, 75.54, and 79.56 and assigned to (111), (200), (220), (311), and (222), respectively. The peaks are indexed to NiO (JCPDS card no. 78-0643). XRD of NiCoO_x without Fe and a Ni-to-Co ratio of 2:1 is also added for comparison. We performed a detailed study in our previous work with NiCoO_x catalysts for OER and AEM electrolysis; the XRD of NiCoO_x with a different Ni-to-Co ratio can be reviewed in that study [23].

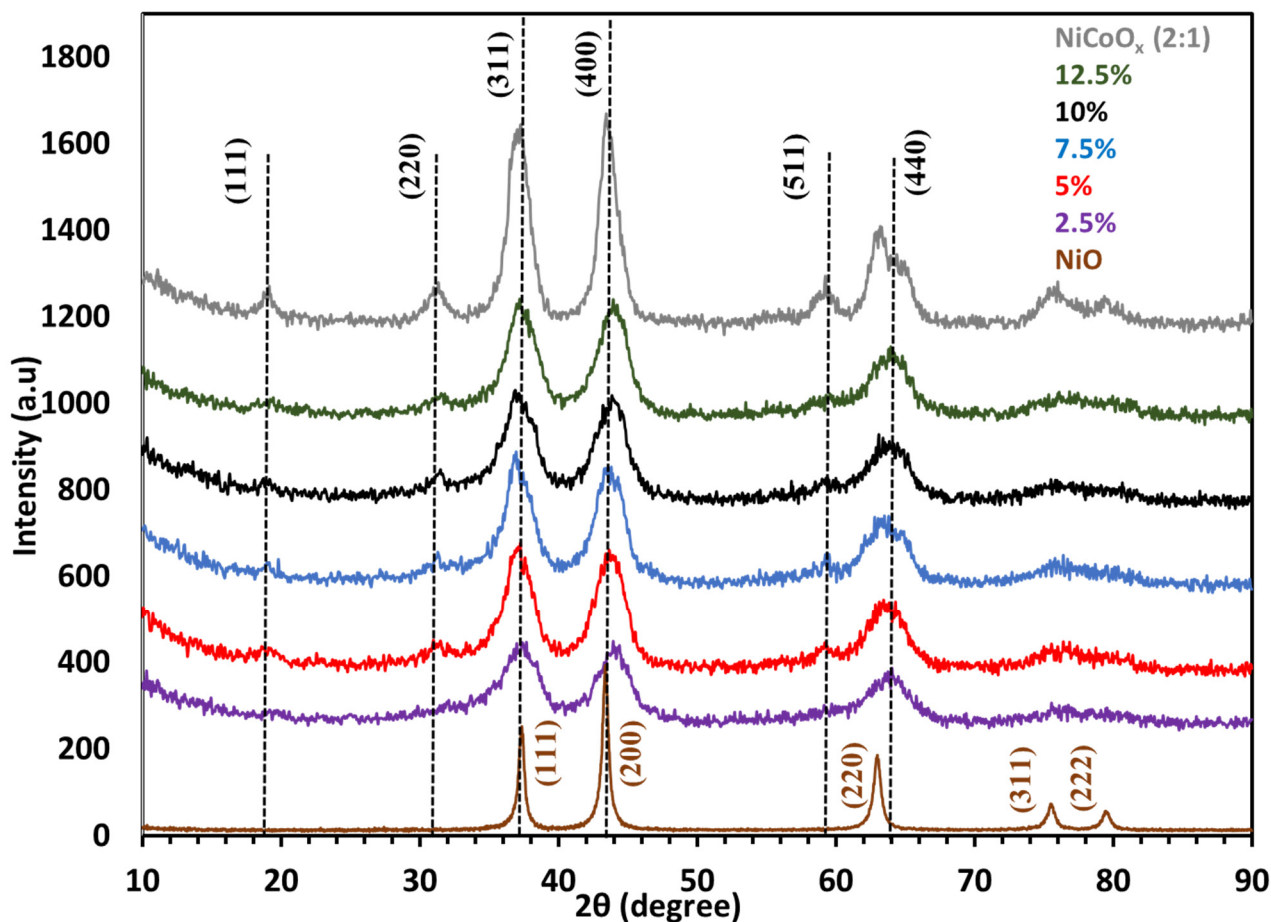


Figure 2. XRD of NiFeCoO_x catalysts with a Fe content of 2.5 to 12.5% wt.%.

Other studies have shown that with a lower Fe content in a co-precipitated NiFeO_x catalyst with 15% Fe loading, there was no XRD peak observed for NiFe₂O₄ or Fe₂O₃ [24]. For the XRD of the Ni/NiFe₂O₄ catalyst, no XRD peak due to NiFe₂O₄ was observed at the Fe mol% of 10 to 15%. At a higher mol% of 25, the XRD at peak at $2\theta \approx 35^\circ$ was observed, and a further increase in the Fe mol% to 50 resulted in the appearance of Fe₂O₃ diffraction peaks [25].

2.1. Oxygen Evolution Reaction

To evaluate the catalytic activity of the NiFeCoO_x catalysts, LSV was performed in 1M KOH. NiFeCoO_x (5%Fe) showed the highest catalytic activity with an overpotential of 228 mV at a current density of 10 mA cm⁻², as shown in Figure 3a, in all cases, the catalyst was coated on the nickel foam. The catalytic activity increased in the order of 5% > 7.5% > 2.5% > 10% > 12.5% with respect to total Fe content. The trend showed maximum activity at 5% and 7.5% Fe content, which decreases after further addition of Fe content to 10% and 12.5% Fe. Similar results were reported for NiFeO_x electrocatalysts, where the OER activity improved until 15% Fe content, and with a further increase in Fe content to 30%, the OER activity decreased [13]. A higher Fe content in NiFe layered double hydroxide (LDH) material is reported to decrease OER activity because of the formation of the FeO_xH_y segregated phase, which decreases the electrical conductivity of the catalysts [26].

NiO catalysts have shown comparatively lower activity for OER [21,27], there is a self-redox peak at 1.45 V (V vs. RHE) that is indicative of Ni²⁺ to Ni³⁺ oxidation. With the increase in Fe content higher than 5% Fe, the peak became less prominent. In earlier work, it has been proposed that the addition of Fe in NiO materials promotes charge transfer and increases the valence state of Ni. This made further oxidation of the catalyst relatively difficult, causing the disappearance of Ni²⁺ to the Ni³⁺ peak at 1.45 V. This

partial charge transfer between Ni and Fe has been linked to improved OER activity [28]. Figure 3b shows the overpotential at current densities of 10, 50, and 100 mA cm⁻². At 10 mA cm⁻², the overpotential did not change much with the increase in Fe content in the NiFeCoO_x catalyst series, where the NiFeCoO_x (5% Fe) catalyst had an overpotential of 228 mV at 10 mA cm⁻². At higher current densities of 50 mA cm⁻² and 100 mA cm⁻², the overpotential of NiFeCoO_x (5% Fe) was 406 and 495 mV, which is the lowest among other catalysts, and with a further increase in Fe content to 12.5%, it increased to 458 mV and 558 mV for 50 mA cm⁻² and 100 mA cm⁻², respectively.

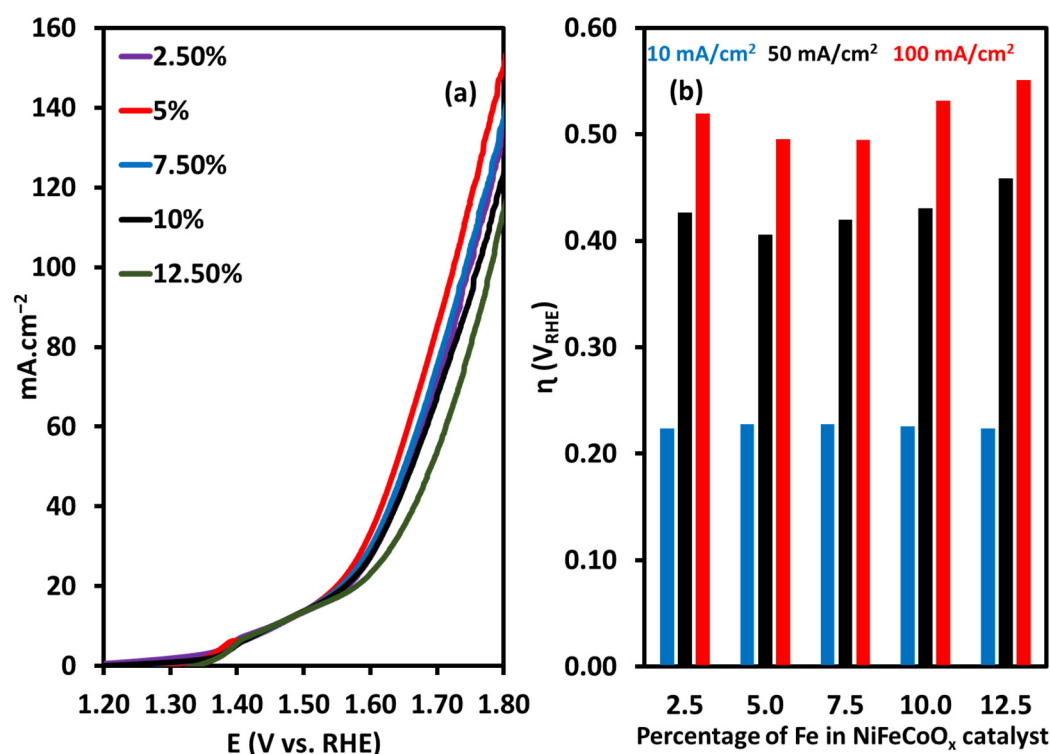


Figure 3. Oxygen evolution reaction for the NiFeCoO_x catalyst series in 1M KOH. (a) Polarization curves (85% iR-corrected) of NiFeCoO_x catalysts. (b) Overpotential of the OER at 10, 50, and 100 mA/cm².

The kinetics of the NiFeCoO_x catalysts were compared by using a Tafel plot, as shown in Figure 4a. The catalysts with 5%, 7.5%, and 12.5% showed a lower Tafel slope, which indicates faster reaction kinetics of the OER on these catalysts. A long-term stability test was performed on the NiFeCoO_x (5% Fe) catalyst for 100 h, as shown in Figure 4b. The OER catalyst stability test was performed at a current density of 50 mA/cm². During the 100 h operation, the voltage increased from 1.741 V to 1.79 V (vs. RHE). The rate of voltage increase over the 100 h stability period was 0.49 mV/h. This test helped to analyze the stability of the catalyst for a prolonged OER at a relatively higher current density.

The determination of double-layer capacitance (C_{dl}) involved conducting cyclic voltammetry (CV) in the non-faradic region, specifically ranging from 0.967 V to 1.167 V. The plots in Figure 5a–f depict the relationship between the scan rate and current density in the non-faradic region. C_{dl} was calculated from the slope of the scan rate vs. the current density plot, as shown in Figure 6. The table in Figure 6 shows the values of C_{dl} and ECSA for the NiFeCoO_x catalysts. The calculated values for the ECSA were 172.5 cm², 127.5 cm², 132.5 cm², 135 cm², and 132.5 cm² for the NiFeCoO_x catalysts with Fe concentrations of 2.5%, 5%, 7.5%, 10%, and 12.5%, respectively.

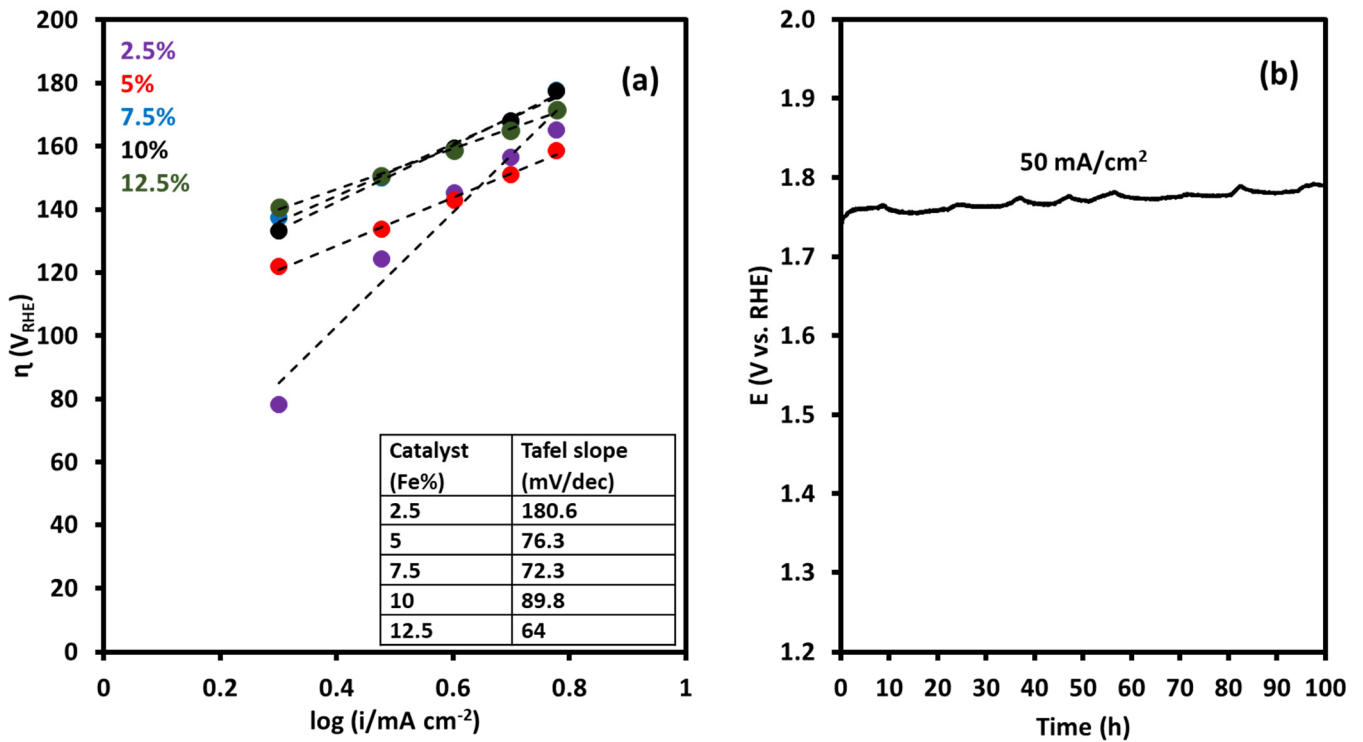


Figure 4. (a) Tafel plots for the OER with NiFeCoO_x catalysts in 1 M KOH. (b) Long-term OER tests of the NiFeCoO_x (5%Fe) catalyst at 50 mA/cm².

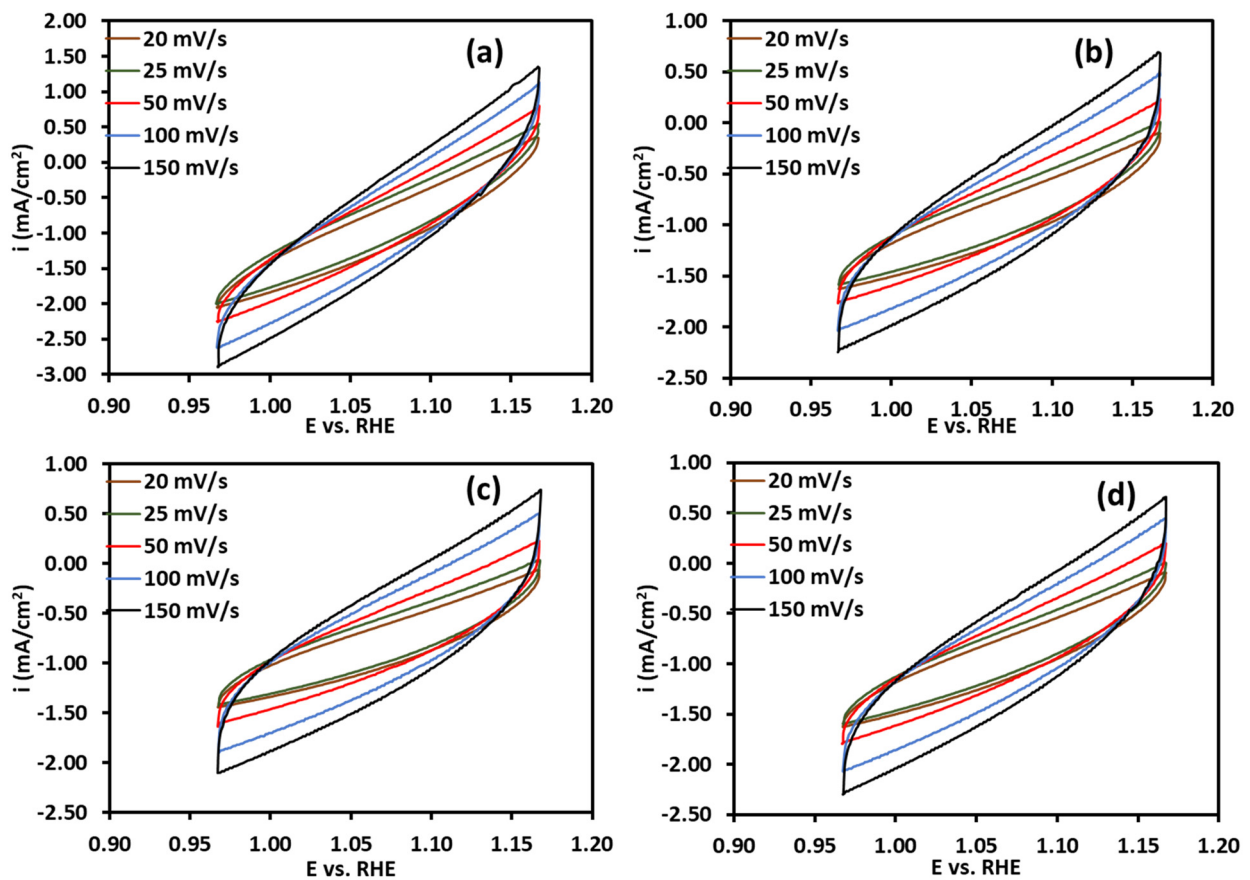


Figure 5. Cont.

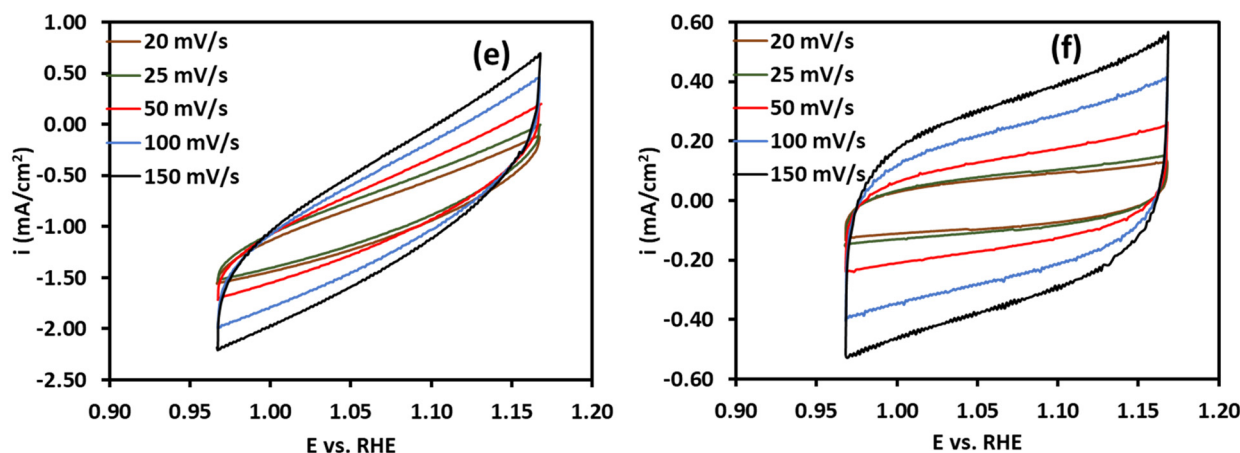


Figure 5. Cyclic voltammetry for the determination of C_{dl} for NiFeCoO_x catalysts with varying Fe contents of (a) 2.5%, (b) 5%, (c) 7.5%, (d) 10%, (e) 12.5%, and (f) NiCo(OH)_x (5%).

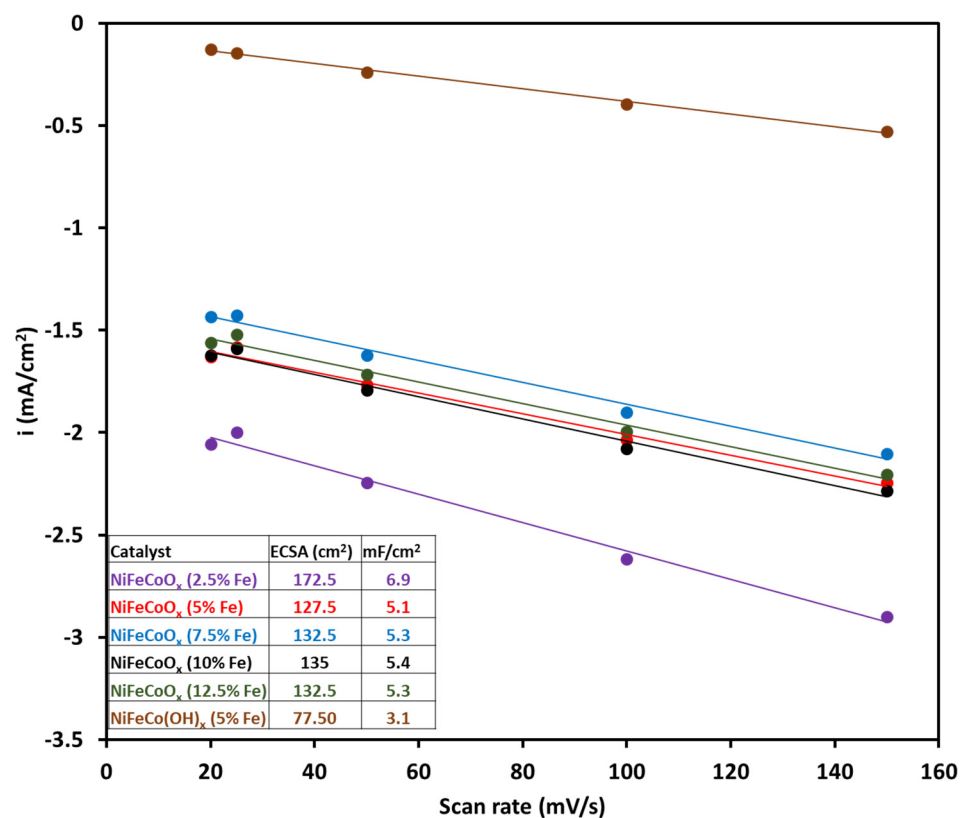


Figure 6. Plot of scan rate vs. current density for the evaluation of the electrochemical double-layer capacitance (C_{dl}) of NiFeCoO_x catalysts.

2.2. Single-Cell Performance with the NiFeCoO_x Catalyst

The activity of the catalyst in the AEM electrolyzer was tested using chronoamperometry. Figure 7 shows the activity of the catalyst at 45 °C, with voltage ranges from 1.5 V to 2.2 V. The voltage was constant for one minute at each voltage. The electrolyzer performance was monitored, and there was very little variation in current density at a fixed voltage. At a voltage of 2.2 V, the maximum current density was 1675 mA cm⁻².

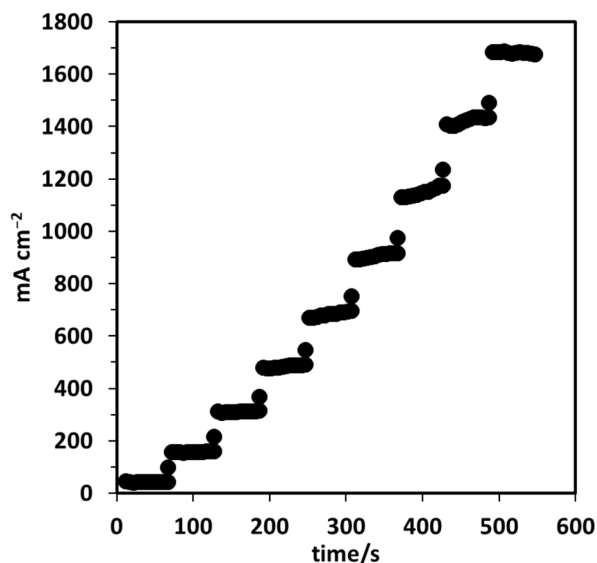


Figure 7. NiFeCoO_x (5% Fe) catalyst activity measurement in the AEM electrolyzer using chronoamperometry at 45 °C with a voltage from 1.5 to 2.3 V.

Figure 8a shows polarization curves for the series of NiFeCoO_x catalysts at 45 °C. The Ni-to-Co ratio in all the catalysts was 2:1 with Fe content changed from 2.5 to 12.5%. The catalyst with 5% Fe content showed the highest activity of 1128 mA cm⁻² at 2.1 V. Other catalysts also exhibited increased activity, with the catalyst containing 7.5 wt% Fe achieving a current density of 832 mA cm⁻² at the same voltage. As the percentage of iron (Fe) exceeded 7.5 wt%, a reduction in activity was observed, particularly at concentrations of 10 and 12.5 wt%.

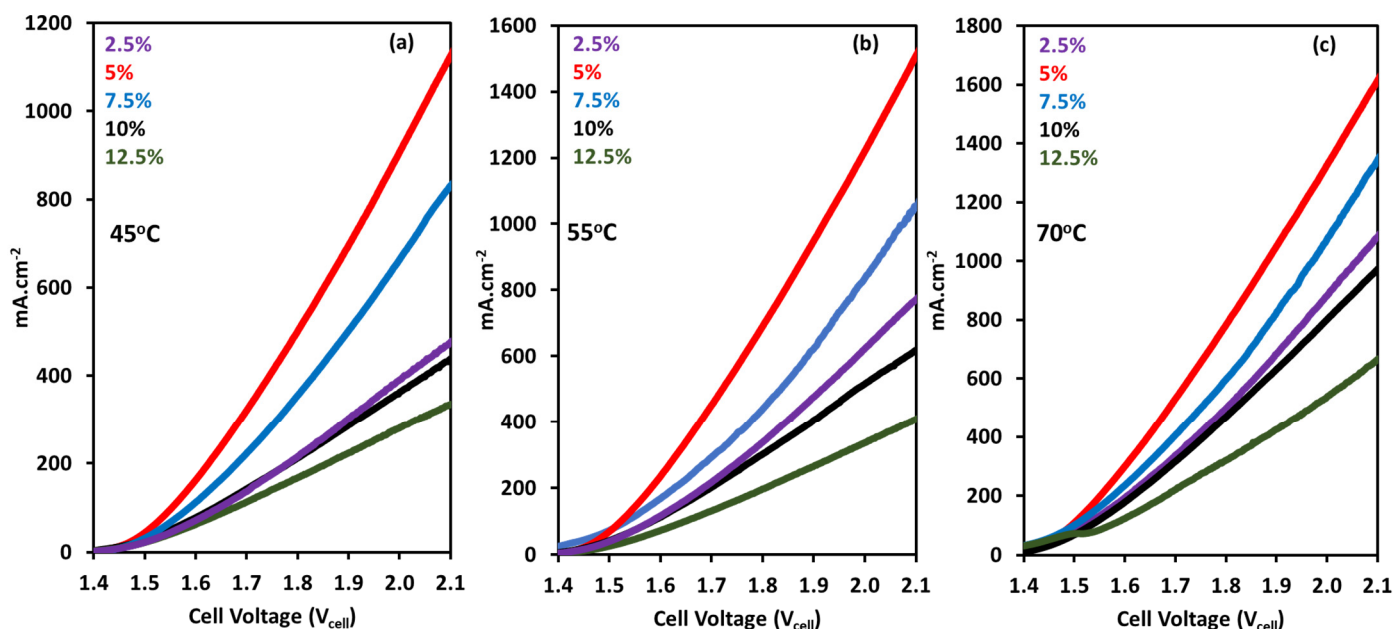


Figure 8. Linear sweep voltammetry was conducted across different temperatures using the X-37-50 T membrane for AEM electrolysis at (a) 45 °C, (b) 55 °C, and (c) 70 °C. The cathode employed Pt/C, while the anode utilized a synthesized NiFeCoO_x catalyst with a varying Fe content ranging from 2.5% to 12.5% wt.%.

AEM water electrolysis is usually performed at higher temperatures than 45 °C, the reason is to improve the reaction kinetics and to increase the conductivity of the electrolyte. Figure 8b,c show the AEM electrolysis performance at 55 °C and 70 °C. The

trend in activity was the same with 5% Fe, having the highest current density of 1516 and 1620 mA cm⁻² at 55 °C and 70 °C, respectively, at 2.1 V. With the 7.5 wt% Fe catalyst, the highest activities were 1048 and 1340 mA cm⁻² at 55 °C and 70 °C, respectively. An increase in temperature can have a positive effect on the overall activity of electrolysis by decreasing the overpotential (the extra energy required to drive a reaction) at the cathode and anode [7].

In our earlier work, it was found that a NiFeCoO_x catalyst performed well compared with a NiO catalyst for AEM water electrolysis [24]. The formation of a spinel phase, such as NiCo₂O₄, can be a contributing factor to enhancing the activity in electrocatalysis, particularly for the oxygen evolution reaction. The presence of Fe oxides can also promote the formation of the NiCo₂O₄ spinel phase, which is known to be a good oxygen evolution electrocatalyst [29]. The optimum percentage of Fe in Ni-based catalysts for the OER has been shown to vary in different studies. For a NiO/NiFe₂O₄-based mixed oxide catalyst, the OER activity was reported to be maximum at 10 mol% of Fe with 90% of Ni. Increasing the Fe content to 20 mol%, the activity of the OER decreased to half. It was proposed that the formation of amorphous Fe₂O₃ could be the reason for the lower activity with the increase in Fe content [25]. In another study, it was shown that the addition of Fe in a Ni hydroxide catalyst enhanced the overall performance of alkaline water electrolysis, with higher Fe content, the performance was reported to decrease [30]. A nickel iron oxide with a sputtered catalyst with 1.9% Fe was reported to have a lower overpotential than a 5.6% Fe catalyst for the OER [31].

A variety of materials and compositions have been studied for their application in the OER under alkaline conditions. Among these, transition metals have proven to be highly effective, demonstrating both elevated activity and stability in such environments [32]. Catalysts containing nickel (Ni), iron (Fe), and cobalt (Co) have proven to be effective in reducing the overpotential necessary for the OER [33–36]. Investigations have been carried out on the suitability of transition metal oxides, hydroxides, and oxyhydroxides as catalysts for the OER. The general pattern among these catalysts indicates that Ni-based catalysts exhibit the highest activity, followed by Co and then Fe [20,21]. By incorporating transition metals into metal oxides or hydroxides, the dynamics of interactions among metallic phases change because of the modification of d-d intermetallic bonding. This causes a reduction in the energy required for intermediates to adsorb, leading to low adsorption energy of intermediates and thereby faster reaction kinetics [37,38].

In this work, the addition of Fe in NiCoO_x catalysts showed a promotional effect on the overall activity of the catalyst when the Fe content was 5 to 7.5%. The increased activity is linked to the improved conductivity of the catalyst and also the decrease in the overpotential of the OER catalyst. The NiO catalyst's performance for the OER has been demonstrated to be enhanced by a Fe content between 10 and 20%. Co aids in the formation of Ni³⁺, and it was suggested that Fe would stabilize Ni in the Ni²⁺ oxidation state [14]. In another study, trimetallic Ni_{0.6}Co_{0.2}Fe_{0.2} was reported to have a current density of 1.5 A/cm² at 2 V. The enhancement in the activity of the catalysts was due to the Ni(OH)₂ to NiOOH transformation at relatively lower temperature [39].

Figure 9a shows a bar graph, which illustrates a clear electrolysis activity trend with the change in Fe content under the condition of 2.1 V at 55 °C. At 2.5 wt% Fe, the catalyst activity is higher than the 10 and 12.5% Fe, which means that a higher Fe content retards the overall activity. The optimum Fe content was at 5 and 7.5%, which shows the highest activity among the series of catalysts. For comparison, when the Fe content increased from 2.5 to 5%, the current density increased by 96%.

An Arrhenius plot was used to calculate the apparent activation energy for AEM water electrolysis by plotting the logarithm of current density and reciprocal temperature, as shown in Figure 9b. The apparent activation energy was calculated at a voltage range of 1.5 to 2.2 V and a temperature range of 45 to 70 °C. The apparent activation energy was in the range of –33.09 to –12.40 kJ/mol for the NiFeCoO_x catalyst with 5% Fe content. Table 1 shows the apparent activation energy at each current density, the activation energy

decreased with the increase in the voltage. In electrochemical reactions, such as the OER, as voltage increases, the potential energy of the reactants also increases. This increase in potential energy can be used to overcome the activation energy barrier required for the reaction to occur, making it easier for the reaction to take place [23,40].

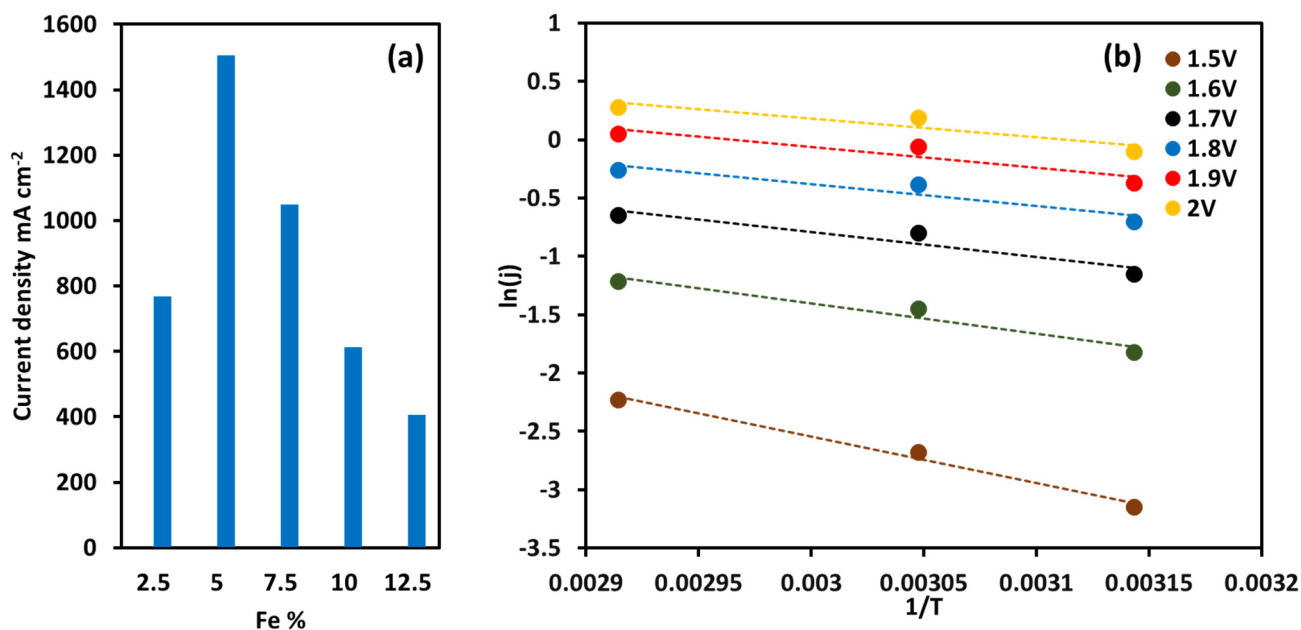


Figure 9. (a) Trend in the activity of AEM electrolysis performance with an increase in the Fe content at 2.1 V and 55 °C. (b) Arrhenius plot of the NiFeCoO_x (5% Fe) catalyst as the anode for AEM water electrolysis at a temperature range of 45–70 °C.

Table 1. Apparent activation energy with the NiFeCoO_x (5% Fe) catalyst at the anode for AEM water electrolysis.

Voltage (V)	Activation Energy (kJ/mol)
1.5	−33.09
1.6	−21.66
1.7	−17.63
1.8	−15.62
1.9	−14.94
2	−13.36
2.1	−12.57
2.2	−12.40

2.3. Electrochemical Impedance Spectroscopy

EIS is a robust technique employed for investigating the operational characteristics of electrolyzer cells, especially in the context of AEM water electrolysis cells [41,42]. By this analysis, the impedance of the electrolyzer during the electrolysis operation can be measured. In addition, the impedance at the cathode and anode and resistance due to electrolytes and the membrane can also be evaluated [43]. The data obtained from the EIS measurements can be analyzed by Nyquist plots, which allow for the visualization of the impedance characteristics of the cell. A Nyquist plot can be used to identify different components of the impedance, such as the charge-transfer resistance and the Warburg impedance [44].

Figure 10 illustrates the Nyquist plot obtained during the electrolysis operation at 55 °C, performed at a voltage of 1.7 V, for the NiFeCoO_x catalyst series. On the Nyquist plot, the x-intercept at the high-frequency region signifies the ohmic resistance (R_{ohm}), and the activation resistance (R_{act}) can be determined by subtracting the first x-intercept from the second x-intercept. The Nyquist plot in Figure 10 illustrates that the semicircle diameter for NiFeCoO_x with a 5% loading is smaller than that of the other catalysts with different Fe loadings. This suggests that the activation resistance for this catalyst is comparatively lower when compared with the other catalysts.

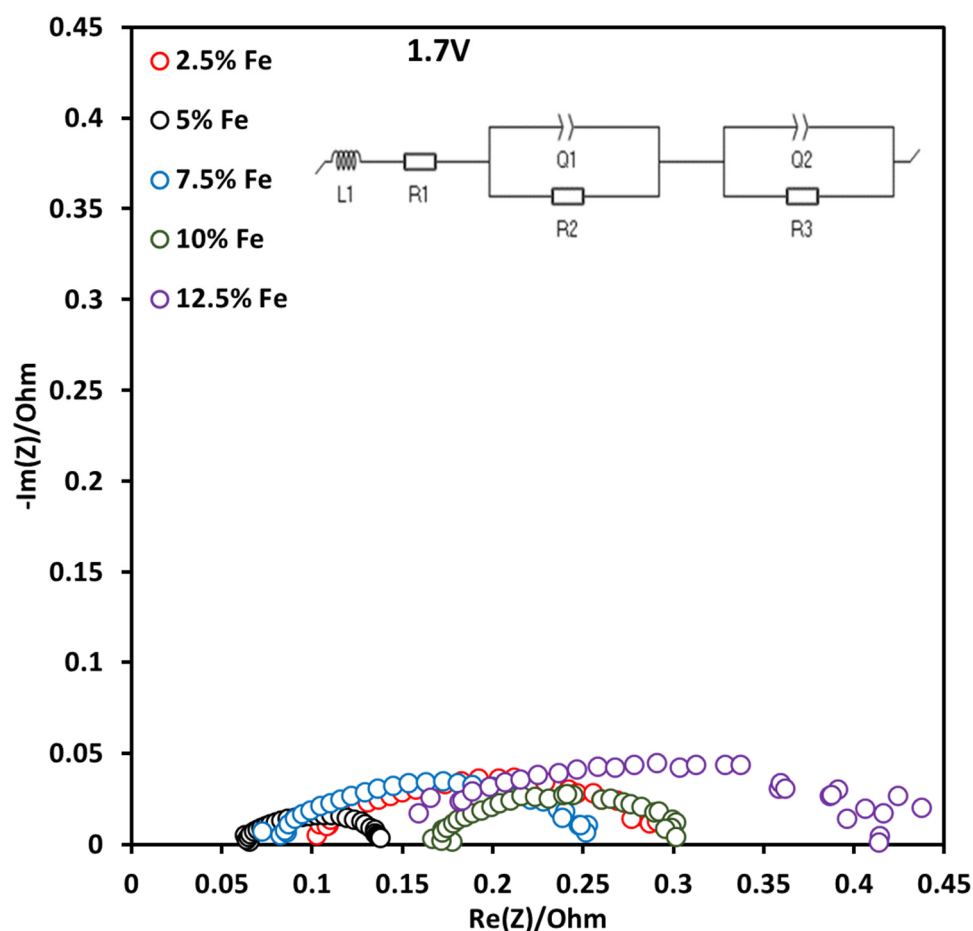


Figure 10. EIS analysis with a Nyquist plot at 1.7 V for AEM electrolysis with NiFeCoO_x catalysts at 55 °C.

To gain further insight into the performance of the electrolyzer cell, equivalent circuit fitting was used to analyze the contributions of different components to the impedance. An equivalent circuit is shown in Figure 10 with different electrolyzer components, where (L) is inductance, R1 is the ionic resistance, R2 and R3 are the activation resistances, and Q2 and Q3 are the constant phase elements (CPEs) (Q2 and Q3) at the electrodes [23]. Because of the non-uniform nature of the electrodes, CPEs were used instead of capacitive elements Q [45].

Table 2 shows the activation resistance and ohmic resistance evaluated from the Nyquist plots for the catalyst series during AEM electrolysis. The Nyquist plots showed the same trends as those observed in the performance testing, where the activation resistance and ohmic resistance increased in the same order of 5%Fe < 7.5%Fe < 2.5% Fe < 10% Fe < 12.5% Fe. The lower activation resistance (0.074 Ω) and ohmic resistance (0.064 Ω) for the NiFeCoO_x (5% Fe) catalyst resulted in higher performance for the AEM electrolysis. The lower ohmic resistance for NiFeCoO_x (5% Fe) was due to the increased conductivity of the catalyst because of the addition of Fe. The higher loading of Fe greater than 5%

resulted in a decrease in the conductivity of the catalyst and resulted in an increase in ohmic resistance. Similarly, a higher Fe content in the catalyst resulted in increased activation resistance, which means that the OER at the anode has a lower overpotential on NiFeCoO_x (5% Fe) than the other catalysts in the series. These results clearly showed that the addition of Fe in the range of 5–7.5% in the NiCoO_x catalyst increased the catalyst conductivity, leading to a reduction in ohmic resistance. The activation resistance was also lower for the catalysts with 5–7.5% Fe content, and these catalysts showed higher current densities in single-cell performance.

Table 2. Resistances evaluated from equivalent circuit fitting. EIS was performed at 55 °C and 1.7 V.

Catalyst Fe%	Ohmic Resistance	Activation Resistance	Membrane Resistance
	R_{ohm} (Ω)	$R_{anode} + R_{cathode}$ (Ω)	$R_{membrane}$ (Ω)
2.5	0.102	0.218	0.090
5	0.064	0.074	0.060
7.5	0.083	0.180	0.078
10	0.166	0.139	0.167
12.5	0.159	0.284	0.137

Potentiostatic EIS was also used to study the effect of temperature on different resistances involved in the AEM electrolysis operation. EIS was performed on the NiFeCoO_x (5% Fe) catalyst from 45 to 70 °C at 1.7 V and 2 V, as shown in Figure 11. The equivalent circuit fitting results in Table 3 suggest that as the temperature of the AEM electrolyzer increases, the ohmic resistance decreases, which can improve the overall efficiency of the electrolysis process.

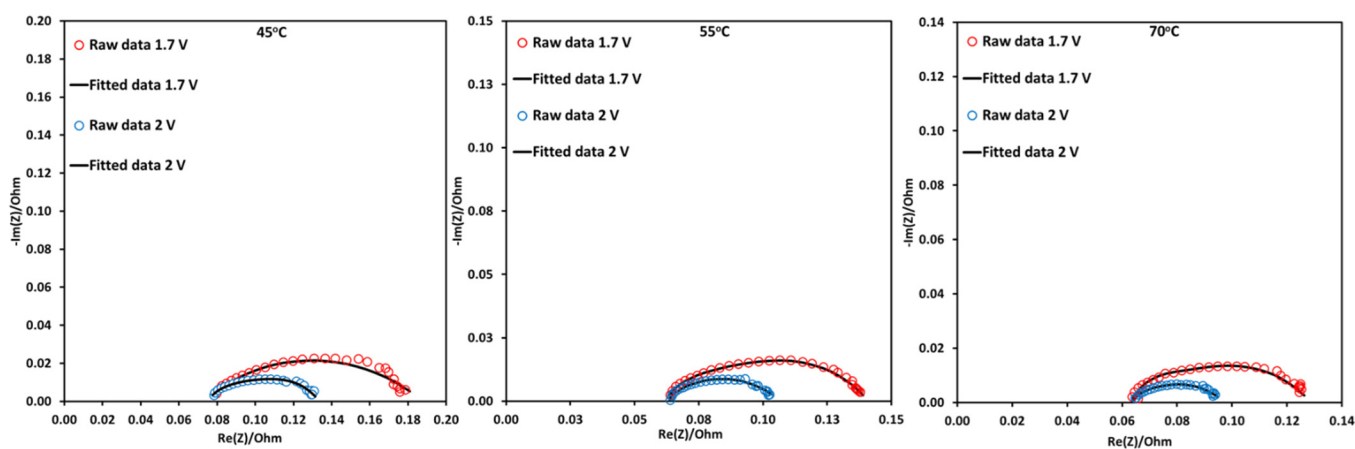


Figure 11. Effect of temperature on AEM water electrolysis with EIS analysis using Nyquist plots at three distinct temperatures (45 °C, 55 °C, and 70 °C). The NiFeCoO_x catalyst with (5 wt% Fe) was used at the anode for AEM water electrolysis. EIS was performed at 1.7 V and 2 V.

The results in Table 3 show that with an increase in temperature from 45 to 70 °C, the total activation resistance at the anode and cathode decreased from 0.096 to 0.065 Ω at 1.7 V and from 0.051 to 0.029 Ω at 2 V. With the increase in the voltage from 1.7 to 2 V, the activation resistance decreased at each temperature. The activation resistance at 45 °C, 55 °C, and 70 °C decreased by 46.8%, 47.3%, and 55.3% by increasing the voltage to 2 V.

Table 3. Equivalent circuit results for EIS analysis. AEM electrolysis was carried out at 1.7 V and 2 V from 45 °C to 70 °C with the NiFeCoO_x (5 wt% Fe) anode.

Temperature	Ohmic Resistance R _{ohm} (Ω)	Activation Resistance R _{anode} + R _{cathode} (Ω)	Membrane Resistance R _{membrane} (Ω)
45 °C	0.080	0.096	0.072
55 °C	0.064	0.074	0.060
70 °C	0.060	0.065	0.058
2 V			
45 °C	0.078	0.051	0.071
55 °C	0.064	0.039	0.060
70 °C	0.061	0.029	0.060

2.4. Comparison of the NiFeCoO_x Catalyst with NiFeCo(OH)_x

Ni-based hydroxide-based materials have shown good stability in alkaline conditions and are known to have high OER activity. Ni-, Fe-, and Co-based layered double hydroxide materials are also reported to have high OER activity [26,46,47]. The synthesis method for NiFeCo(OH)_x was similar to NiFeCoO_x, with the only difference being that it was not annealed at a high temperature, and the catalyst was dried at room temperature for one day. The loading of Fe was 5%, and the performance of the catalyst was compared with the NiFeCoO_x (5% Fe) catalyst. The XRD pattern of NiFeCo(OH)_x revealed peaks that corresponded to reflections of a hydrotalcite-like structure, as shown in Figure 12, with distinct peaks at 2θ at 10.4, 21, 34, 38.5, and 60 which were assigned to (003), (006), (012), (015), and (110) reflections and indexed to (JCPDS: 00-035-0965).

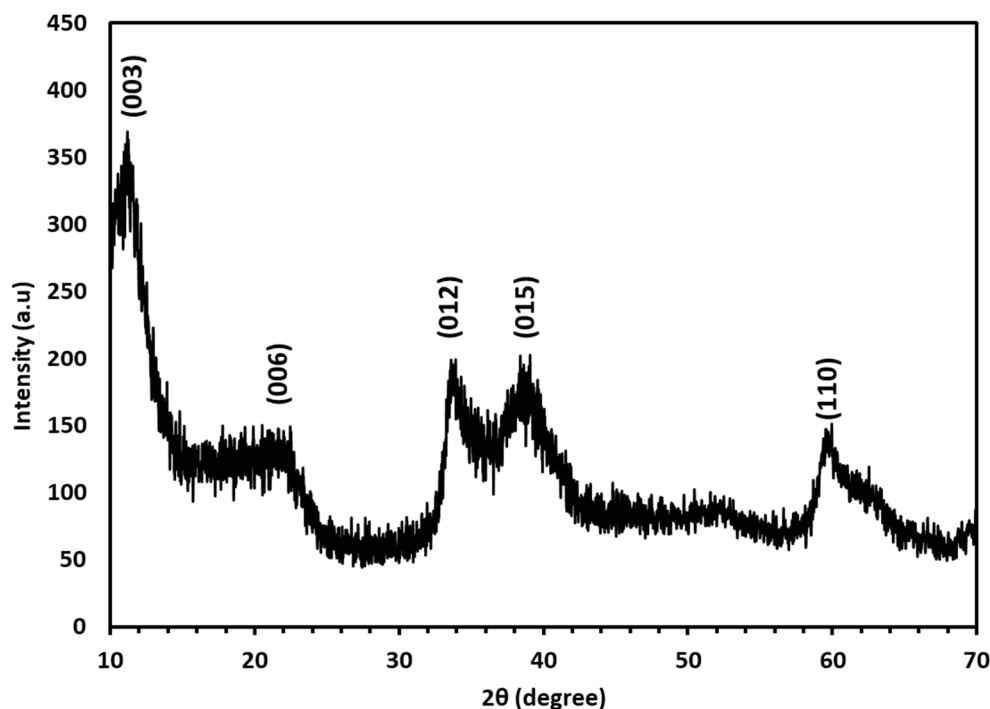


Figure 12. XRD of the NiFeCo(OH)_x catalyst with 5 wt% Fe.

To compare the electrolyzer activity of NiFeCo(OH)_x and NiFeCoO_x, a dioxide membrane X-37-50 T was employed, and the MEA preparation method followed the previously described procedure. The operation was conducted at three temperatures (45 °C, 55 °C, and 70 °C), as depicted in Figure 13a–c. At each temperature, the NiFeCo(OH)_x catalyst

exhibited a lower current density compared with NiFeCoO_x, with both catalysts having the same loading of 25 mg cm⁻². At a voltage of 2.2 V, the current density for NiFeCo(OH)_x was 514 mA cm⁻² at 45 °C, 588 mA cm⁻² at 55 °C, and 617 mA cm⁻² at 70 °C. In contrast, for the NiFeCoO_x catalyst, the current density was higher, reaching 1311 mA cm⁻² at 45 °C, 1800 mA cm⁻² at 55 °C, and 1880 mA cm⁻² at 70 °C. The activity of NiFeCo(OH)_x was higher as it achieved a current density higher than 500 mA cm⁻² at each temperature, but compared with NiFeCoO_x, the activity was 2.5 times lower at 45 °C. At relatively higher temperatures of 55 °C and 70 °C, the NiFeCo(OH)_x activity was 3 times lower than the NiFeCoO_x catalyst. The hydroxide form of the OER catalyst is reported to show higher activities in the literature. However, their low electronic conductivity can be a limitation for the OER. This means that the electrons may have difficulty moving through the material, which can slow down the reaction and decrease the efficiency of the electrolysis process [46]. The hydroxyl group present in the catalyst results in oxygen defects. It is reported that the presence of oxygen defects can change the properties of materials, including energy levels and conductivity. It also leads to an increase in the number of reactive and surface-active sites. However, an overabundance of oxygen vacancies causes a deformation in the metal–oxygen bond, which decreases the electron transfer between the catalyst surface and the intermediate in the oxygen evolution reaction [26].

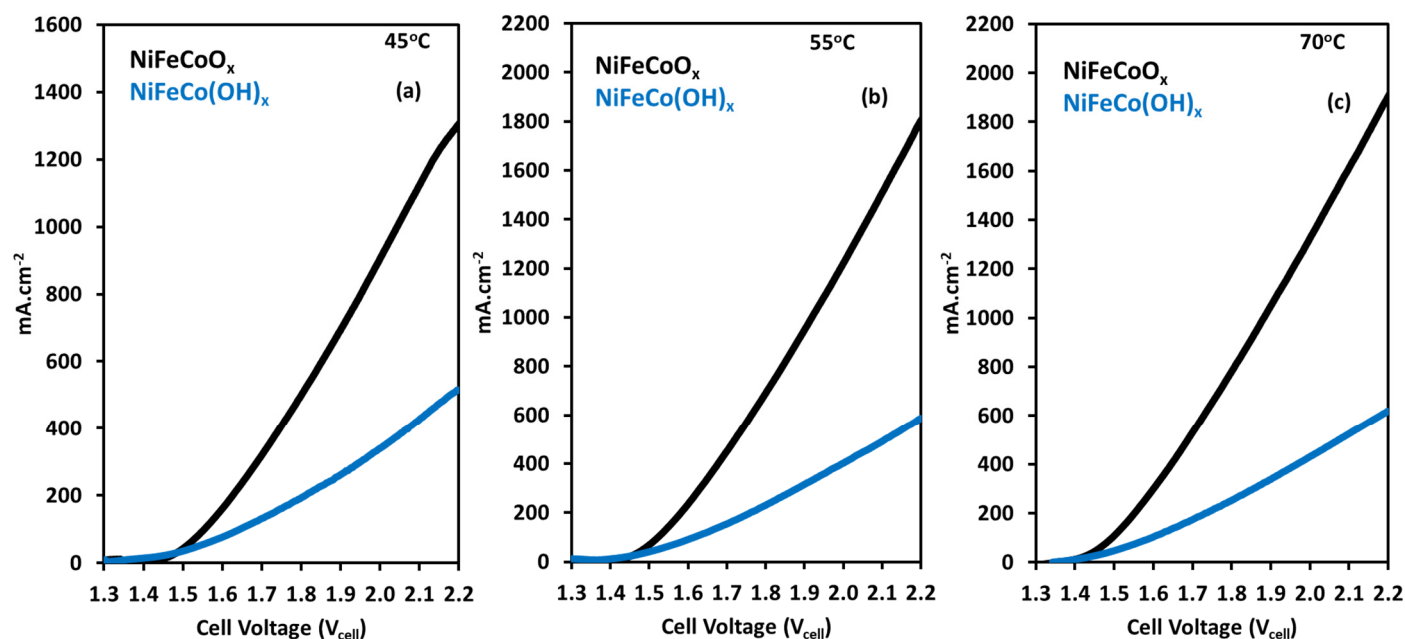


Figure 13. Electrolysis performance using NiFeCoO_x and NiFeCo(OH)_x with 5 wt% Fe at a temperature range of (a) 45 °C, (b) 55 °C, (c) 70 °C.

Modifications to nickel hydroxide catalysts to improve their performance for OER typically focus on several key areas. Heteroatom doping, such as the incorporation of Fe and Co into a catalyst, can enhance the conductivity of the material and promote charge transfer, thereby improving its OER performance [48–50]. Heteroatomic doping, specifically Fe-doping, has been shown to be a promising method for improving the activity of nickel-based (oxy)hydroxide catalysts in the OER. Studies have found that the intentional and/or incidental incorporation of Fe into nickel (oxy)hydroxide can significantly enhance the catalytic activity of the material. It was reported that the introduction of Fe into nickel (oxy)hydroxide catalysts affects the electronic structure of the material and promotes a partial charge transfer activation on the Ni atoms. Fe-doping in nickel (oxy)hydroxide catalysts has been found to result in optimal adsorption energy for oxygen intermediates, making the OER more efficient. Other research has also suggested that the Fe ions, rather than the Ni sites, may be the active sites for the generation of O₂ from intermediate species on Ni_{1-x}Fe_xOOH catalysts [51].

Another strategy to improve the activity of NiFe-based layered double hydroxides (LDHs) in the OER is a ternary metal catalyst. This can affect the conductivity and structure of a binary catalyst (NiFe hydroxide), leading to enhanced OER activity. For instance, ternary NiFeCo mixed metal oxide film has been found to exhibit enhanced OER activity compared with reference NiFe LDH catalysts. This approach can create new active sites and change the electronic structure of a catalyst, leading to improved performance in the OER [14,47]. Some synergism has been reported between Ni and Co in the $\text{Ni}(\text{Co})\text{O}_x\text{H}_y$ catalyst for the OER, which is more active than the corresponding CoO_xH_y catalyst. The OER activity was reported to increase by 3 times by co-deposition of Fe in $\text{Ni}(\text{Co})\text{O}_x\text{H}_y$ [52].

The lower conductivity of layered double hydroxides (LDHs) has been a barrier to their use as catalysts in the OER. To overcome this limitation, researchers have attempted to combine LDHs with conductive materials such as reduced graphene oxide (rGO) and carbon nanotubes (CNTs) or to grow LDHs on conductive substrates such as nickel foam or carbon fiber cloth. This approach aims to enhance the conductivity of the catalysts, making them more efficient in the OER process [53–55].

Figure 14a shows EIS results at 55 °C for the $\text{NiFeCo}(\text{OH})_x$ (5% Fe) catalyst using the X-37-50 T membrane. The ohmic resistances at 1.7 and 2 V were 0.225 Ω and 0.218 Ω , and the activation resistances were 0.244 Ω and 0.2 Ω , as determined from equivalent circuit fittings. When these EIS results were compared with NiFeCoO_x (5% Fe) for electrolysis operation, and the ohmic resistances were 3.5 and 3.4 times higher for the $\text{NiFeCo}(\text{OH})_x$ catalyst. This could be due to the low conductivity offered by this catalyst, which offered higher resistance in electron transport. The conductivity also affected the overall performance of the electrolyzer, and this catalyst achieved a lower current density than the NiFeCoO_x catalyst during water electrolysis at the same conditions. The activation resistances were also 3.29 and 5.1 times higher compared with the NiFeCoO_x catalyst. This explains the lower performance of hydroxide catalysts for water electrolysis compared with the other NiFeCoO_x series of catalysts.

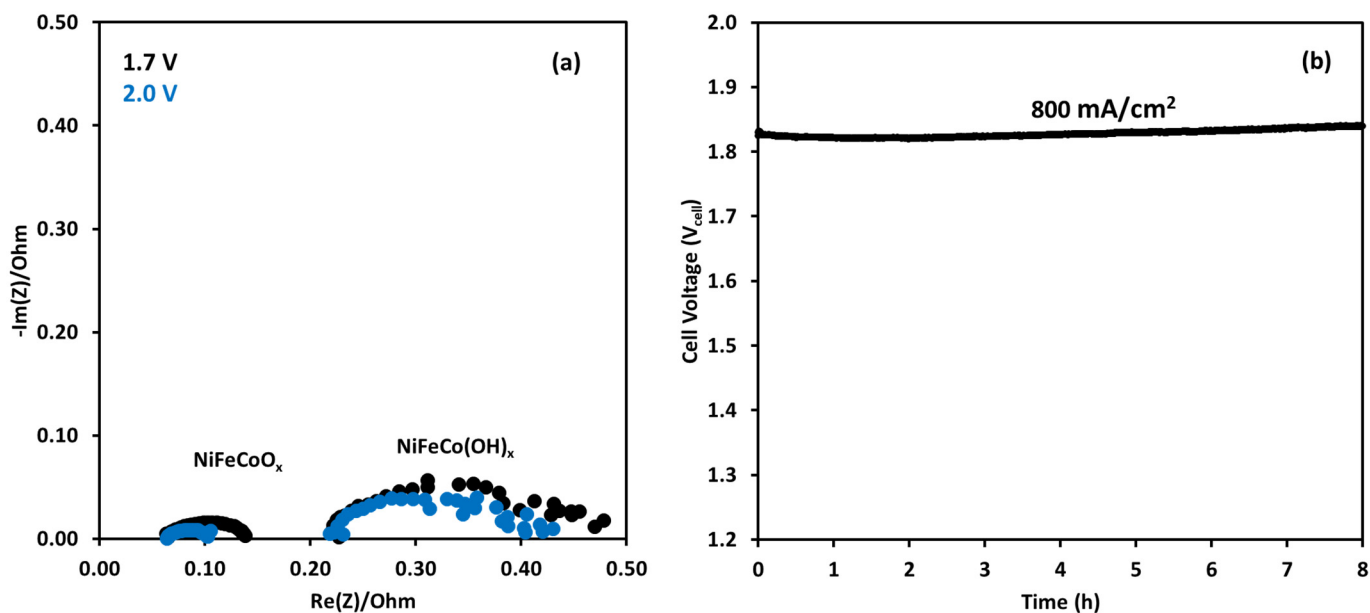


Figure 14. (a) Comparison of the Nyquist plot for NiFeCoO_x and $\text{NiFeCo}(\text{OH})_x$ catalysts with 5 wt% Fe at 55 °C for AEM water electrolysis. (b) AEM electrolyzer durability test at 800 mA/cm^2 for 8 h in 1M KOH; the electrolyzer was operated at 55 °C.

2.5. AEM Electrolyzer Durability Test

A durability test was performed for water electrolysis with the NiFeCoO_x (5%Fe) OER catalyst at 800 mA/cm^2 for 8 h. Cell efficiencies were determined within the first hour of the stability test. The cell efficiency was 70.5% at this high current density operation.

During the stability testing, the voltage did not increase much during the analysis. The degradation rate observed during the test was 2.3 mV/h. The initial voltage at the start of the test was 1.825 V, and after 8 h, it reached 1.839 V, as shown in Figure 14b. The Faradic efficiency was also calculated within the first 60 min of the operation, with an efficiency of 87%.

One of the factors that affect electrolyzer performance in longer runs is the stability of AEM. Some of the commercially available membranes tested in the durability testing were not stable even at very low current density; for example, the FAA-3 membrane was reported to degrade within 10 h of the operation at 20 mA cm⁻². With aryl ether-free HMT-PBI, AEM showed stability for 200 h at a current density of 25 mA cm⁻² [56]. Higher current density AEM stability tests were reported with FAS-50 and Sustainions X-37-50 membranes at 60 °C, where both membranes showed stability for 180 h and 2000 h at 1 A cm⁻² [57].

3. Experimental

3.1. Synthesis of the NiFeCoO_x Catalyst

For the catalyst synthesis, nickel nitrate (Ni(NO₃)₂), cobalt nitrate Co(NO₃)₂·6H₂O, and iron nitrate Fe(NO₃)₂ were utilized as precursors for Ni, Co, and Fe, respectively. By maintaining a Ni-to-Co molar ratio of 2:1, the Fe concentration varied from 2.5 to 12.5 wt% per metal basis. All three precursors were dissolved in water at 25 °C, and 1 M NaOH was then added dropwise for 60 min during the precipitation phase, followed by 2 h of stirring. The resulting catalyst suspension underwent centrifugation to isolate the solid catalyst, which was thoroughly washed to remove excess NaOH. The washed solids were dried in an oven overnight and subsequently subjected to calcination at 300 °C for 5 h in a furnace to convert the catalyst into its metal oxide form.

3.2. The Oxygen Evolution Reaction (OER) in the Three-Electrode System

The three-electrode OER system was made by using graphite as the counter electrode, a Standard Calomel Electrode (SCE) as the reference electrode, and the NiFeCoO_x catalyst coated on nickel foam as the working electrode. Linear sweep voltammetry (LSV) and cyclic voltammetry (CV) were performed using a potentiostat (VMP-3, Biologic). The working electrode surface area was 1 cm², and 1M KOH was used as an electrolyte at room temperature. OER activity polarization curves were recorded with a scan rate of 5 mV/s and 85% iR correction. Durability tests were performed at a constant current density of 50 mA cm⁻² for 100 h. CV was used in non-faradic regions to determine the double-layer capacitance (C_{dl}). The electrochemical surface area (ECSA) was estimated by dividing C_{dl} by the smooth plane capacitance (C_s), with a specified value of 40 μF/cm².

All potentials were converted to values relative to the reversible hydrogen electrode (RHE) using the Nernst equation. Catalyst loading was maintained at 5 mg·cm⁻² for each run, and the catalyst was coated onto the nickel foam using catalyst slurry prepared from the catalyst, 5 wt% Nafion solution, and isopropanol.

3.3. Fabrication of the Gas Diffusion Electrode

Nickel foam with a thickness of 1.7 mm was used as the gas diffusion layer (GDL) for the anode. The catalyst was coated by forming a slurry using a catalyst, Nafion solution (Nafion™ 1100W from Sigma Aldrich, St. Louis, MO, USA), water, and isopropanol. The Nafion content was 10 wt% of the total catalyst amount. For all AEM electrolysis tests, the catalyst loading at the anode was 25 mg·cm⁻².

A Pt/C catalyst (40 wt%, HISPEC 4000, Johnson Matthey, London, UK) was used for the cathode side. A coating of 1 mg of Pt was applied to carbon paper (Sigracet 29BC) using an airbrush. The Nafion content was 20 wt% of the catalyst in the ink used for depositing the Pt/C catalyst. After fabrication of the gas diffusion electrodes, a membrane electrode assembly (MEA) was made by inserting an anion exchange membrane (AEM, dioxide membrane X-37-50 grade T, San Diego, CA, USA) between the anode and cathode.

The MEA assembly involved placing a porous transport layer (made by pressing three nickel foams to a thickness of 2 mm) into the casing, followed by inserting a nickel foam anode, the AEM, and then the carbon paper cathode. The total active area of the MEA was 3.24 cm^2 with dimensions $1.8 \text{ cm} \times 1.8 \text{ cm}$ [23].

3.4. AEM Electrolyzer Performance Test

The operation was performed by using LSV and chronoamperometry. A potentiostat connected with 100 A Booster VMP3B-100 (Biologic, Seyssinet-Pariset, France) was used for analysis, 1 M KOH was used as an electrolyte, which was circulated with a flow rate of 90 mL/min , and the temperature range used in electrolysis was from 45 to $70 \text{ }^\circ\text{C}$. EIS was performed at the voltage range of 1.7 V to 2 V , with a frequency range of 100 kHz to 100 mHz . The data were analyzed by Nyquist plots.

The durability of the AEM electrolyzer was tested at a constant current density of 0.8 A/cm^2 for 8 h. To calculate cell efficiency, which is the ratio of power input to the electrolyzer to the power of hydrogen out, the AEM electrolyzer power was calculated by multiplying the cell voltage and current density. Cell efficiency was calculated by using Equation (1). Faradaic efficiency was determined by measuring the quantity of hydrogen generated at room temperature.

$$\text{Cell efficiency (\%)} = \frac{\text{moles of hydrogen} \times \Delta H \times 100}{\text{AEM electrolyzer power input}} \quad (1)$$

Figure 15a depicts an AEM water electrolyzer with water and oxygen outlets on the anode side and a hydrogen outlet on the cathode side. The electrolyzer employs an anion exchange membrane to separate the anode and cathode. The 1M KOH solution was circulated only from the anode side.

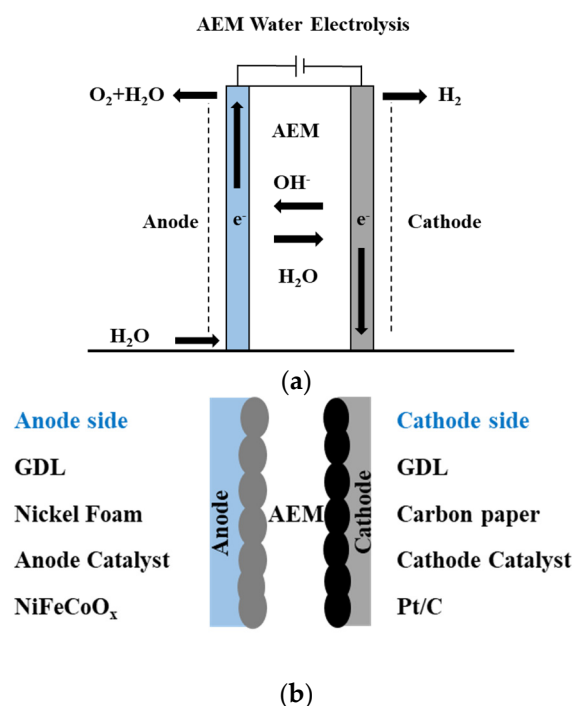


Figure 15. (a) Configuration of the AEM water electrolyzer. (b) Schematic of the membrane electrode assembly used in this study.

The water reduction reaction at the cathode generates hydrogen, while hydroxyl ions move through the membrane and are oxidized at the anode to release oxygen. Figure 15b shows the schematic of the MEA, where NiFeCoO_x was used in the nickel foam and Pt/C was used in the carbon paper gas diffusion layer.

4. Conclusions

In this study, the catalytic activity of NiFeCoO_x catalysts in AEM water electrolysis was investigated. NiFeCoO_x catalysts exhibited a well-defined NiCo₂O₄ spinel crystal structure. The electrochemical analysis in the three-electrode system revealed that the catalytic activity of the NiFeCoO_x catalysts varied with the Fe content. Specifically, the catalyst with 5% Fe content exhibited the highest catalytic activity, achieving an overpotential of 228 mV at a current density of 10 mA cm². The long-term stability testing for 100 h showed stable performance with a slight voltage increase, which shows the stability of the NiFeCoO_x catalyst anode for the OER. As the Fe content increased beyond the optimal concentration, the catalytic activity gradually decreased. This observation suggests that there is an optimal Fe concentration for maximizing the catalyst's performance, beyond which the presence of excess Fe might negatively affect catalytic activity because of the decrease in the conductivity of the catalyst and increase in the overpotential of the catalyst. This finding emphasizes the importance of careful control over the catalyst composition to achieve optimal performance. The single-cell tests conducted under practical operating conditions further supported the superior electrochemical activity of the NiFeCoO_x catalyst with 5% Fe content. This catalyst consistently demonstrated the highest current densities of 1516 mA cm⁻² and 1620 mA cm⁻² at 55 °C and 70 °C, respectively, at 2.1 V, highlighting its stability and suitability for real-world applications. NiFeCoO_x consistently exhibited higher current density than the NiFeCo(OH)_x catalyst at each temperature, with the former achieving 2.5 times higher activity at 45 °C and three times higher activity at 55 °C and 70 °C. These results indicate that NiFeCoO_x outperforms NiFeCo(OH)_x in terms of electrolyzer activity, particularly at elevated temperatures.

EIS coupled with equivalent circuit fitting analysis of various catalyst compositions in AEM water electrolyzers shows performance characteristics. The catalyst study during AEM electrolysis revealed that NiFeCoO_x (5% Fe) exhibited superior performance, attributed to its lower activation and ohmic resistances. Increasing the temperature demonstrated a steady decrease in overall resistances, enhancing electrolysis efficiency. A higher voltage further lowered the activation resistance, emphasizing the importance of voltage and temperature in optimizing AEM electrolysis.

The durability test of the NiFeCoO_x (5%Fe) OER catalyst in water electrolysis showed promising results. The catalyst demonstrated stable performance throughout the 8-hour AEM electrolysis at 800 mA cm⁻², suggesting its reliability and durability in high current density operations. The cell efficiency measured during the initial hour of the stability test was 70.5%, highlighting the catalyst's efficiency in facilitating water electrolysis and hydrogen generation. The faradic efficiency of the system was measured to be 87% during the first hour of operation, indicating efficient electrochemical reactions during water electrolysis.

These findings have important implications for the development of efficient and sustainable hydrogen production. By optimizing the composition of NiFeCoO_x catalysts, it is possible to enhance the electrochemical performance of alkaline water electrolysis systems, thereby facilitating the production of hydrogen in a more environmentally friendly and economically viable manner.

Supplementary Materials: The following supporting information can be downloaded at: <https://www.mdpi.com/article/10.3390/catal14050322/s1>.

Author Contributions: K.W.A.: conceptualization, methodology, data curation, writing—original draft, and visualization. M.F.: conceptualization, methodology, supervision, project administration, and funding acquisition. All authors have read and agreed to the published version of the manuscript.

Funding: This work was supported by the Department of Chemical Engineering at the University of Waterloo, Canada Research Chair Tier I—Zero-emission Vehicles and Hydrogen Energy Systems Grant number: 950-232215, and The Natural Sciences and Engineering Research Council of Canada (NSERC), Discovery Grants Program, RGPIN-2020-04149.

Data Availability Statement: Data are contained within the article and supplementary materials.

Conflicts of Interest: The authors declare that they have no known competing financial interests or personal relationships that could have appeared to influence the work reported in this paper.

References

1. Vincent, I.; Bessarabov, D. Low cost hydrogen production by anion exchange membrane electrolysis: A review. *Renew. Sustain. Energy Rev.* **2018**, *81*, 1690–1704. [[CrossRef](#)]
2. Miller, H.A.; Bouzek, K.; Hnat, J.; Loos, S.; Bernäcker, C.I.; Weißgärber, T.; Röntzsch, L.; Meier-Haack, J. Green hydrogen from anion exchange membrane water electrolysis: A review of recent developments in critical materials and operating conditions. *Sustain. Energy Fuels* **2020**, *4*, 2114–2133. [[CrossRef](#)]
3. Ahmed, K.W.; Jang, M.J.; Park, M.G.; Chen, Z.; Fowler, M. Effect of Components and Operating Conditions on the Performance of PEM Electrolyzers: A Review. *Electrochem* **2022**, *3*, 581–612. [[CrossRef](#)]
4. Carmo, M.; Fritz, D.L.; Mergel, J.; Stolten, D. A comprehensive review on PEM water electrolysis. *Int. J. Hydrogen Energy* **2013**, *38*, 4901–4934. [[CrossRef](#)]
5. Li, C.; Baek, J.-B. The promise of hydrogen production from alkaline anion exchange membrane electrolyzers. *Nano Energy* **2021**, *87*, 106162. [[CrossRef](#)]
6. López-Fernández, E.; Sacedón, C.G.; Gil-Rostra, J.; Yubero, F.; González-Elipe, A.R.; de Lucas-Consuegra, A. Recent advances in alkaline exchange membrane water electrolysis and electrode manufacturing. *Molecules* **2021**, *26*, 6326. [[CrossRef](#)]
7. Vincent, I.; Kruger, A.; Bessarabov, D. Development of efficient membrane electrode assembly for low cost hydrogen production by anion exchange membrane electrolysis. *Int. J. Hydrogen Energy* **2017**, *42*, 10752–10761. [[CrossRef](#)]
8. Yang, J.; Jang, M.J.; Zeng, X.; Park, Y.S.; Lee, J.; Choi, S.M.; Yin, Y. Non-precious electrocatalysts for oxygen evolution reaction in anion exchange membrane water electrolysis: A mini review. *Electrochem. Commun.* **2021**, *131*, 107118. [[CrossRef](#)]
9. McCrory, C.C.; Jung, S.; Peters, J.C.; Jaramillo, T.F. Benchmarking heterogeneous electrocatalysts for the oxygen evolution reaction. *J. Am. Chem. Soc.* **2013**, *135*, 16977–16987. [[CrossRef](#)]
10. McCrory, C.C.; Jung, S.; Ferrer, I.M.; Chatman, S.M.; Peters, J.C.; Jaramillo, T.F. Benchmarking hydrogen evolving reaction and oxygen evolving reaction electrocatalysts for solar water splitting devices. *J. Am. Chem. Soc.* **2015**, *137*, 4347–4357. [[CrossRef](#)]
11. Singh, A.; Singh, R. Effect of V substitution at B-site on the physicochemical and electrocatalytic properties of spinel-type NiFe₂O₄ towards O₂ evolution in alkaline solutions. *Int. J. Hydrogen Energy* **2010**, *35*, 3243–3248.
12. Hardin, W.G.; Mefford, J.T.; Slanac, D.A.; Patel, B.B.; Wang, X.; Dai, S.; Zhao, X.; Ruoff, R.S.; Johnston, K.P.; Stevenson, K.J. Tuning the electrocatalytic activity of perovskites through active site variation and support interactions. *Chem. Mater.* **2014**, *26*, 3368–3376. [[CrossRef](#)]
13. Qi, J.; Zhang, W.; Xiang, R.; Liu, K.; Wang, H.; Chen, M.; Han, Y.; Cao, R. Porous nickel–iron oxide as a highly efficient electrocatalyst for oxygen evolution reaction. *Adv. Sci.* **2015**, *2*, 1500199. [[CrossRef](#)] [[PubMed](#)]
14. Bates, M.K.; Jia, Q.; Doan, H.; Liang, W.; Mukerjee, S. Charge-transfer effects in Ni–Fe and Ni–Fe–Co mixed-metal oxides for the alkaline oxygen evolution reaction. *ACS Catal.* **2016**, *6*, 155–161. [[CrossRef](#)]
15. Gerken, J.B.; Shaner, S.E.; Massé, R.C.; Porubsky, N.J.; Stahl, S.S. A survey of diverse earth abundant oxygen evolution electrocatalysts showing enhanced activity from Ni–Fe oxides containing a third metal. *Energy Environ. Sci.* **2014**, *7*, 2376–2382. [[CrossRef](#)]
16. Li, Y.-F.; Selloni, A. Mechanism and activity of water oxidation on selected surfaces of pure and Fe-doped NiO_x. *ACS Catal.* **2014**, *4*, 1148–1153. [[CrossRef](#)]
17. Dinh, K.N.; Zheng, P.; Dai, Z.; Zhang, Y.; Dangol, R.; Zheng, Y.; Li, B.; Zong, Y.; Yan, Q. Ultrathin porous NiFeV ternary layer hydroxide nanosheets as a highly efficient bifunctional electrocatalyst for overall water splitting. *Small* **2018**, *14*, 1703257. [[CrossRef](#)] [[PubMed](#)]
18. Jin, Y.; Huang, S.; Yue, X.; Du, H.; Shen, P.K. Mo- and Fe-modified Ni(OH)₂/NiOOH nanosheets as highly active and stable electrocatalysts for oxygen evolution reaction. *ACS Catal.* **2018**, *8*, 2359–2363. [[CrossRef](#)]
19. Bo, X.; Li, Y.; Hocking, R.K.; Zhao, C. NiFeCr hydroxide holey nanosheet as advanced electrocatalyst for water oxidation. *ACS Appl. Mater. Interfaces* **2017**, *9*, 41239–41245. [[CrossRef](#)]
20. Subbaraman, R.; Tripkovic, D.; Chang, K.-C.; Strmcnik, D.; Paulikas, A.P.; Hirunsit, P.; Chan, M.; Greeley, J.; Stamenkovic, V.; Markovic, N.M. Trends in activity for the water electrolyser reactions on 3dM(Ni,Co,Fe,Mn)hydr(oxy)oxide catalysts. *Nat. Mater.* **2012**, *11*, 550–557. [[CrossRef](#)]
21. Trotochaud, L.; Young, S.L.; Ranney, J.K.; Boettcher, S.W. Nickel–iron oxyhydroxide oxygen-evolution electrocatalysts: The role of intentional and incidental iron incorporation. *J. Am. Chem. Soc.* **2014**, *136*, 6744–6753. [[CrossRef](#)] [[PubMed](#)]
22. Poudel, M.B.; Kim, H.J. Confinement of Zn–Mg–Al-layered double hydroxide and α-Fe₂O₃ nanorods on hollow porous carbon nanofibers: A free-standing electrode for solid-state symmetric supercapacitors. *Chem. Eng. J.* **2022**, *429*, 132345. [[CrossRef](#)]
23. Ahmed, K.W.; Habibpour, S.; Chen, Z.; Fowler, M. Investigation of NiCoOx catalysts for anion exchange membrane water electrolysis: Performance, durability, and efficiency analysis. *J. Energy Storage* **2024**, *79*, 110149. [[CrossRef](#)]
24. Ahmed, K.W.; Jang, M.J.; Habibpour, S.; Chen, Z.; Fowler, M. NiFeOx and NiFeCoOx Catalysts for Anion Exchange Membrane Water Electrolysis. *Electrochem* **2022**, *3*, 843–861. [[CrossRef](#)]

25. Landon, J.; Demeter, E.; Inoglu, N.; Keturakis, C.; Wachs, I.E.; Vasic, R.; Frenkel, A.I.; Kitchin, J.R. Spectroscopic characterization of mixed Fe–Ni oxide electrocatalysts for the oxygen evolution reaction in alkaline electrolytes. *ACS Catal.* **2012**, *2*, 1793–1801. [[CrossRef](#)]
26. Park, Y.S.; Jeong, J.-Y.; Jang, M.J.; Kwon, C.-Y.; Kim, G.H.; Jeong, J.; Lee, J.; Lee, J.; Choi, S.M. Ternary layered double hydroxide oxygen evolution reaction electrocatalyst for anion exchange membrane alkaline seawater electrolysis. *J. Energy Chem.* **2022**, *75*, 127–134. [[CrossRef](#)]
27. Gao, M.; Sheng, W.; Zhuang, Z.; Fang, Q.; Gu, S.; Jiang, J.; Yan, Y. Efficient water oxidation using nanostructured α -nickel-hydroxide as an electrocatalyst. *J. Am. Chem. Soc.* **2014**, *136*, 7077–7084. [[CrossRef](#)] [[PubMed](#)]
28. Louie, M.W.; Bell, A.T. An investigation of thin-film Ni–Fe oxide catalysts for the electrochemical evolution of oxygen. *J. Am. Chem. Soc.* **2013**, *135*, 12329–12337. [[CrossRef](#)]
29. Guerrini, E.; Piozzini, M.; Castelli, A.; Colombo, A.; Trasatti, S. Effect of FeO_x on the electrocatalytic properties of NiCo₂O₄ for O₂ evolution from alkaline solutions. *J. Solid State Electrochem.* **2008**, *12*, 363–373. [[CrossRef](#)]
30. Li, X.; Walsh, F.C.; Pletcher, D. Nickel based electrocatalysts for oxygen evolution in high current density, alkaline water electrolyzers. *Phys. Chem. Chem. Phys.* **2011**, *13*, 1162–1167. [[CrossRef](#)]
31. Miller, E.L.; Rocheleau, R.E. Electrochemical behavior of reactively sputtered iron-doped nickel oxide. *J. Electrochem. Soc.* **1997**, *144*, 3072–3077. [[CrossRef](#)]
32. Lu, F.; Zhou, M.; Zhou, Y.; Zeng, X. First-row transition metal based catalysts for the oxygen evolution reaction under alkaline conditions: Basic principles and recent advances. *Small* **2017**, *13*, 1701931. [[CrossRef](#)]
33. Jang, M.J.; Yang, J.; Jeong, J.; Kim, G.H.; Kwon, C.Y.; Myung, N.V.; Lee, K.H.; Choi, S.M. Promotion Effect of Modified Ni/C by La–Ce Oxide for Durable Hydrogen Evolution Reaction. *ACS Sustain. Chem. Eng.* **2021**, *9*, 12508–12513. [[CrossRef](#)]
34. Lyons, M.E.; Brandon, M.P. The oxygen evolution reaction on passive oxide covered transition metal electrodes in alkaline solution. Part II—Cobalt. *Int. J. Electrochem. Sci.* **2008**, *3*, 1425–1462. [[CrossRef](#)]
35. Lyons, M.E.; Brandon, M.P. The oxygen evolution reaction on passive oxide covered transition metal electrodes in alkaline solution. Part III—Iron. *Int. J. Electrochem. Sci.* **2008**, *3*, 1463–1503. [[CrossRef](#)]
36. Lyons, M.E.; Brandon, M.P. The oxygen evolution reaction on passive oxide covered transition metal electrodes in aqueous alkaline solution. Part I—Nickel. *Int. J. Electrochem. Sci.* **2008**, *3*, 1386–1424. [[CrossRef](#)]
37. Diaz-Morales, O.; Ledezma-Yanez, I.; Koper, M.T.; Calle-Vallejo, F. Guidelines for the rational design of Ni-based double hydroxide electrocatalysts for the oxygen evolution reaction. *ACS Catal.* **2015**, *5*, 5380–5387. [[CrossRef](#)]
38. Wang, P.; Lin, Y.; Wan, L.; Wang, B. Autologous growth of Fe-doped Ni(OH)₂ nanosheets with low overpotential for oxygen evolution reaction. *Int. J. Hydrogen Energy* **2020**, *45*, 6416–6424. [[CrossRef](#)]
39. Faid, A.Y.; Barnett, A.O.; Seland, F.; Sunde, S. Ternary NiCoFe nanosheets for oxygen evolution in anion exchange membrane water electrolysis. *Int. J. Hydrogen Energy* **2022**, *47*, 23483–23497. [[CrossRef](#)]
40. Zegeye, T.A.; Chen, W.-T.; Hsu, C.-C.; Valinton, J.A.A.; Chen, C.-H. Activation energy assessing potential-dependent activities and site reconstruction for oxygen evolution. *ACS Energy Lett.* **2022**, *7*, 2236–2243. [[CrossRef](#)]
41. Siracusano, S.; Trocino, S.; Briguglio, N.; Baglio, V.; Aricò, A.S. Electrochemical impedance spectroscopy as a diagnostic tool in polymer electrolyte membrane electrolysis. *Materials* **2018**, *11*, 1368. [[CrossRef](#)] [[PubMed](#)]
42. Garcia-Navarro, J.C.; Schulze, M.; Friedrich, K.A. Measuring and modeling mass transport losses in proton exchange membrane water electrolyzers using electrochemical impedance spectroscopy. *J. Power Sources* **2019**, *431*, 189–204. [[CrossRef](#)]
43. Kang, Z.; Mo, J.; Yang, G.; Retterer, S.T.; Cullen, D.A.; Toops, T.J.; Green Jr, J.B.; Mench, M.M.; Zhang, F.-Y. Investigation of thin/well-tunable liquid/gas diffusion layers exhibiting superior multifunctional performance in low-temperature electrolytic water splitting. *Energy Environ. Sci.* **2017**, *10*, 166–175. [[CrossRef](#)]
44. Xie, Z.; Holdcroft, S. Polarization-dependent mass transport parameters for orr in perfluorosulfonic acid ionomer membranes: An EIS study using microelectrodes. *J. Electroanal. Chem.* **2004**, *568*, 247–260. [[CrossRef](#)]
45. Ye, Z.-G.; Meng, H.-M.; Sun, D.-B. Electrochemical impedance spectroscopic (EIS) investigation of the oxygen evolution reaction mechanism of Ti/IrO₂+ MnO₂ electrodes in 0.5 m H₂SO₄ solution. *J. Electroanal. Chem.* **2008**, *621*, 49–54. [[CrossRef](#)]
46. Chen, Q.; Yu, Y.; Li, J.; Nan, H.; Luo, S.; Jia, C.; Deng, P.; Zhong, S.; Tian, X. Recent Progress in Layered Double Hydroxide-Based Electrocatalyst for Hydrogen Evolution Reaction. *ChemElectroChem* **2022**, *9*, e202101387. [[CrossRef](#)]
47. Dionigi, F.; Strasser, P. NiFe-based (oxy)hydroxide catalysts for oxygen evolution reaction in non-acidic electrolytes. *Adv. Energy Mater.* **2016**, *6*, 1600621. [[CrossRef](#)]
48. Liu, Z.; Li, N.; Zhao, H.; Zhang, Y.; Huang, Y.; Yin, Z.; Du, Y. Regulating the active species of Ni(OH)₂ using CeO₂: 3D CeO₂/Ni(OH)₂/carbon foam as an efficient electrode for the oxygen evolution reaction. *Chem. Sci.* **2017**, *8*, 3211–3217. [[CrossRef](#)] [[PubMed](#)]
49. Tian, P.; Yu, Y.; Yin, X.; Wang, X. A wafer-scale 1 nm Ni(OH)₂ nanosheet with superior electrocatalytic activity for the oxygen evolution reaction. *Nanoscale* **2018**, *10*, 5054–5059. [[CrossRef](#)]
50. Kim, B.; Oh, A.; Kabiraz, M.K.; Hong, Y.; Joo, J.; Baik, H.; Choi, S.-I.; Lee, K. NiOOH exfoliation-free nickel octahedra as highly active and durable electrocatalysts toward the oxygen evolution reaction in an alkaline electrolyte. *ACS Appl. Mater. Interfaces* **2018**, *10*, 10115–10122. [[CrossRef](#)]
51. Dong, Y.; Zhang, P.; Kou, Y.; Yang, Z.; Li, Y.; Sun, X. A first-principles study of oxygen formation over NiFe-layered double hydroxides surface. *Catal. Lett.* **2015**, *145*, 1541–1548. [[CrossRef](#)]

52. Stevens, M.B.; Enman, L.J.; Korkus, E.H.; Zaffran, J.; Trang, C.D.; Asbury, J.; Kast, M.G.; Toroker, M.C.; Boettcher, S.W. Ternary Ni-Co-Fe oxyhydroxide oxygen evolution catalysts: Intrinsic activity trends, electrical conductivity, and electronic band structure. *Nano Res.* **2019**, *12*, 2288–2295. [[CrossRef](#)]
53. Gong, M.; Li, Y.; Wang, H.; Liang, Y.; Wu, J.Z.; Zhou, J.; Wang, J.; Regier, T.; Wei, F.; Dai, H. An advanced Ni–Fe layered double hydroxide electrocatalyst for water oxidation. *J. Am. Chem. Soc.* **2013**, *135*, 8452–8455. [[CrossRef](#)] [[PubMed](#)]
54. Yin, S.; Tu, W.; Sheng, Y.; Du, Y.; Kraft, M.; Borgna, A.; Xu, R. A Highly Efficient Oxygen Evolution Catalyst Consisting of Interconnected Nickel–Iron-Layered Double Hydroxide and Carbon Nanodomains. *Adv. Mater.* **2018**, *30*, 1705106. [[CrossRef](#)]
55. Tang, C.; Wang, H.; Wang, H.; Zhang, Q.; Tian, G.; Nie, J.; Wei, F. Spatially confined hybridization of nanometer-sized NiFe hydroxides into nitrogen-doped graphene frameworks leading to superior oxygen evolution reactivity. *Adv. Mater.* **2015**, *27*, 4516–4522. [[CrossRef](#)] [[PubMed](#)]
56. Wright, A.G.; Fan, J.; Britton, B.; Weissbach, T.; Lee, H.-F.; Kitching, E.A.; Peckham, T.J.; Holdcroft, S. Hexamethyl-p-terphenyl poly(benzimidazolium): A universal hydroxide-conducting polymer for energy conversion devices. *Energy Environ. Sci.* **2016**, *9*, 2130–2142. [[CrossRef](#)]
57. Liu, Z.; Sajjad, S.D.; Gao, Y.; Yang, H.; Kaczur, J.J.; Masel, R.I. The effect of membrane on an alkaline water electrolyzer. *Int. J. Hydrogen Energy* **2017**, *42*, 29661–29665. [[CrossRef](#)]

Disclaimer/Publisher’s Note: The statements, opinions and data contained in all publications are solely those of the individual author(s) and contributor(s) and not of MDPI and/or the editor(s). MDPI and/or the editor(s) disclaim responsibility for any injury to people or property resulting from any ideas, methods, instructions or products referred to in the content.